

# Differential transcriptome and development of human peripheral plasma cell subsets

Swetha Garimalla,<sup>1</sup> Doan C. Nguyen,<sup>2</sup> Jessica L. Halliley,<sup>3</sup> Christopher Tipton,<sup>4,5</sup> Alexander F. Rosenberg,<sup>6</sup> Christopher F. Fucile,<sup>7</sup> Celia L. Saney,<sup>2</sup> Shuya Kyu,<sup>2</sup> Denise Kaminski,<sup>8</sup> Yu Qian,<sup>9</sup> Richard H. Scheuermann,<sup>9</sup> Greg Gibson,<sup>1</sup> Iñaki Sanz,<sup>4,5</sup> and F. Eun-Hyung Lee<sup>2,5</sup>

<sup>1</sup>School of Biological Sciences, Georgia Institute of Technology, and <sup>2</sup>Division of Pulmonary, Allergy, Critical Care, and Sleep Medicine, Emory University, Department of Medicine, Atlanta, Georgia, USA. <sup>3</sup>Finger Lakes Community College, Rochester, New York, USA. <sup>4</sup>Division of Rheumatology, Emory University, and <sup>5</sup>Lowance Center for Human Immunology in the Departments of Medicine and Pediatrics at Emory University, Atlanta, Georgia, USA. <sup>6</sup>Department of Microbiology and Informatics Institute, University of Alabama, Birmingham, Alabama, USA. <sup>7</sup>Informatics Institute, University of Alabama Birmingham, Alabama, USA. <sup>8</sup>University of Rochester, Rochester, New York, USA. <sup>9</sup>J. Craig Venter Institute, La Jolla, California, USA.

Human antibody-secreting cells (ASCs) triggered by immunization are globally recognized as CD19<sup>lo</sup>CD38<sup>hi</sup>CD27<sup>hi</sup>. Yet, different vaccines give rise to antibody responses of different longevity, suggesting ASC populations are heterogeneous. We define circulating-ASC heterogeneity in vaccine responses using multicolor flow cytometry, morphology, V<sub>H</sub> repertoire, and RNA transcriptome analysis. We also tested differential survival using a human cell-free system that mimics the bone marrow (BM) microniche. In peripheral blood, we identified 3 CD19<sup>+</sup> and 2 CD19<sup>-</sup> ASC subsets. All subsets contributed to the vaccine-specific responses and were characterized by *in vivo* proliferation and activation. The V<sub>H</sub> repertoire demonstrated strong oligoclonality with extensive interconnectivity among the 5 subsets and switched memory B cells. Transcriptome analysis showed separation of CD19<sup>+</sup> and CD19<sup>-</sup> subsets that included pathways such as cell cycle, hypoxia, TNF- $\alpha$ , and unfolded protein response. They also demonstrated similar long-term *in vitro* survival after 48 days. In summary, vaccine-induced ASCs with different surface markers (CD19 and CD138) are derived from shared proliferative precursors yet express distinctive transcriptomes. Equal survival indicates that all ASC compartments are endowed with long-lived potential. Accordingly, *in vivo* survival of peripheral long-lived plasma cells may be determined in part by their homing and residence in the BM microniche.

## Introduction

High-affinity IgG and IgA antibodies provide serological memory that affords protection against previously encountered pathogens. The serologic protection is mediated by long-lived plasma cells (LLPCs), which have been identified in human bone marrow (BM) and the gastrointestinal tract (1–3). Initial response to vaccination is mounted by proliferative antibody-secreting cells (ASCs), which are highly enriched for antigen-specific cells that undergo a massive expansion for approximately 5–14 days after immunization (4–7). Yet, a fundamental gap in understanding remains regarding whether intrinsic programs of the ASC or extrinsic environmental factors determine survival to become an LLPC.

The classic ASC population in blood is based on the relative expression of CD38 and CD27 on CD19<sup>+</sup> cells. However, heterogeneity of the circulating ASC populations has been described extensively (8–12). Characterization of the CD19<sup>+</sup> ASCs has recognized both CD138<sup>+</sup> and CD138<sup>-</sup> populations in the blood after vaccination (4, 9, 12–14) and during steady state (12). Additional markers such as HLA-DR, Ki-67, CD95, and CD126 demonstrate recent activation of the ASCs in the blood after immunization (13). However, by focusing only on CD19<sup>+</sup> ASCs (after excluding CD20<sup>+</sup> cells), the complexity of blood ASC subsets in healthy vaccine responses would not have considered the CD19<sup>-</sup> ASC populations that resemble LLPCs (1). In autoimmune patients, the CD19<sup>-</sup> ASCs appear in the

**Authorship note:** SG, DCN, and JLH are co-first authors.

**Conflict of interest:** FEHL is the founder of MicroBplex, Inc.

**Copyright:** © 2019 American Society for Clinical Investigation

**Submitted:** December 10, 2018

**Accepted:** March 27, 2019

**Published:** May 2, 2019.

**Reference information:** *JCI Insight*. 2019;4(9):e126732. <https://doi.org/10.1172/jci.insight.126732>.

blood of diseased patients during flares (15), and recently, CD19<sup>+</sup>ASCs were also described after vaccination of healthy adults (14). Interestingly, contrary to proposed models of the release of old PCs from BM microniches, the CD19<sup>+</sup> ASC subsets in the blood were shown to have a fraction of new ASCs generated in response to vaccination (14).

The identification of CD19<sup>+</sup>CD38<sup>hi</sup>CD138<sup>+</sup> LLPCs (1) suggests that unique surface markers may play a role in maintaining survival. For example, CD138 was shown to play a direct role in PC survival in mouse models (16). By contrast, the role of CXCR4 in long-lived survival may be related to BM homing rather than intrinsic mechanisms (11). Additionally, loss of markers such as CD19, HLA-DR, and BCR may play a role in survival, although there is little evidence for this observation. Another interpretation for the loss of some markers may actually reflect distinct changes in the intracellular pathways such as G2M checkpoints, metabolism, apoptosis, and autophagy that have been described to sustain LLPCs (1, 17, 18). Nonetheless, it is unclear whether the unique surface markers on heterogeneous ASC populations signify intrinsic differences in cell survival programs.

Germinal center responses play a crucial role in LLPC generation. It is thus possible that specific blood ASCs are imprinted during priming in the germinal center by the local milieu consisting of IL-21 from T follicular helper (T<sub>fh</sub>) cells, follicular dendritic cells, and other T cell help (19–23). Thus, ASC heterogeneity may have evolved to distinguish particular ASC subsets with unique intrinsic mechanisms that are programmed to become long-lived.

In addition to intrinsic mechanisms, extrinsic factors appear to play a critical role in LLPC survival. The BM survival niche plays an important role in the maintenance of LLPCs. The specialized niche that consists of hypoxia, secreted factors from the BM mesenchymal stromal cells (MSCs), and the cytokine APRIL, has recently been shown to maintain human ASCs for over 50 days in culture (24). Whether this environment actually changes the phenotype of the peripheral circulating blood ASCs into LLPCs or merely provides survival factors is still unclear.

In this study, we used FLOW Clustering without K (FLOCK), an automated flow cytometry analysis program (4), to identify 5 distinct populations of ASCs that can be consistently isolated from human blood. Our data validate 3 CD19<sup>+</sup> and 2 newly described CD19<sup>+</sup> ASC populations after vaccination. We also show that the majority of circulating CD138<sup>+</sup> ASCs (both CD19<sup>+</sup> and CD19<sup>+</sup>) are active participants in new vaccine responses and have undergone recent proliferation. Next-generation sequencing (NGS) analysis of the V<sub>H</sub> repertoire shows oligoclonality with a large degree of interconnectivity among the 5 subsets, and despite unique RNA signatures distinguishing populations 2 and 3 (CD19<sup>+</sup>) from population 5 (CD19<sup>+</sup>), those 3 populations have similar long-lived survival potential.

## Results

*Heterogeneity of human ASC subsets in blood.* Human antibody responses after vaccination strongly correlate with a transient increase in circulating ASCs characterized by a CD19<sup>+</sup>CD27<sup>hi</sup>CD38<sup>+</sup> phenotype (4, 25–28). However, the exact contribution of such cells to the long-lived protective antibody production is unclear, in part due to incomplete characterization of the ASC response and over-reliance on the expression of CD19. To address these questions, we performed PBMC fractionation of CD19<sup>+</sup> and CD19<sup>+</sup> populations within CD3<sup>+</sup>CD14<sup>+</sup> cells at the peak of the ASC response after tetanus toxoid and influenza vaccination (6–7 days after immunization) (6). Interestingly, CD19<sup>+</sup> fractions were detected, albeit smaller in frequency than the CD19<sup>+</sup> fractions (Figure 1A). Given the high frequency of vaccine-specific ASCs in both fractions, CD19<sup>+</sup> and CD19<sup>+</sup> cells were analyzed using flow cytometry, yielding 5 putative ASC subsets distinguished by their relative expression of CD38 and CD138; these are population (pop) 1 (CD19<sup>+</sup>CD38<sup>+</sup>CD138<sup>+</sup>), pop 2 (CD19<sup>+</sup>CD38<sup>hi</sup>CD138<sup>+</sup>), pop 3 (CD19<sup>+</sup>CD38<sup>hi</sup>CD138<sup>+</sup>), pop 4 (CD19<sup>+</sup>CD38<sup>hi</sup>CD138<sup>+</sup>), and pop 5 (CD19<sup>+</sup>CD38<sup>hi</sup>CD138<sup>+</sup>) (Figure 1A and Table 1).

We also employed an unbiased automated flow-gating program, FLOCK, with CD19<sup>+</sup> and CD19<sup>+</sup> fractions, and validated these 5 subsets. FLOCK clusters cells in multidimensional hyperdense regions for each of the markers and separates cells into different subsets if they differ from other clusters in at least one marker/dimension. Previously, we identified pop 1 within the CD19<sup>+</sup> fractions using FLOCK (4), although it is a relatively minor fraction of the CD19<sup>+</sup> ASCs. This unsupervised approach revealed no additional ASC subsets for 6 subjects (Supplemental Figure 1 and Supplemental Table 1; supplemental material available online with this article; <https://doi.org/10.1172/jci.insight.126732DS1>), demonstrating that our characterization using CD19, CD38, and CD138 is useful and consistent for elaborating the cellular basis of humoral immune responses.

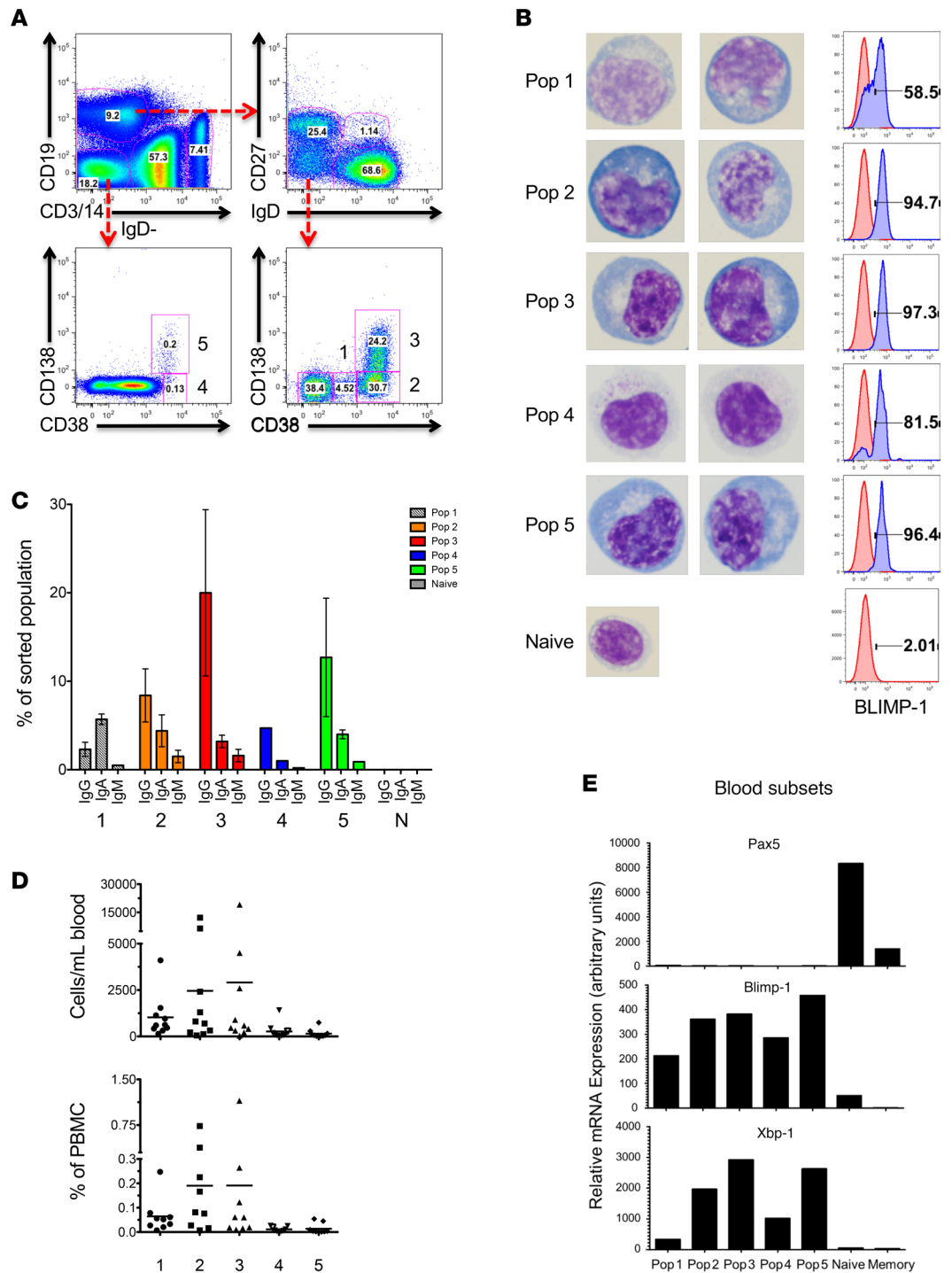


**Figure 1. ASC subsets in human blood 7 days after tetanus vaccination. (A)** Top panels divide the CD19<sup>+</sup> and CD19<sup>-</sup> fractions. Lower panels represent subsets of CD19<sup>-</sup>IgD<sup>-</sup> (left) and CD19<sup>+</sup>IgD<sup>-</sup> (right) fractions. **(B)** Morphology of blood ASC subsets (×100 magnification) by Wright-Giemsa stain. Left column: Sorted blood ASC subsets on day 7 after tetanus vaccination. ASC populations (pops) 1 to 5 and naive B cells are shown. Right column: Percentage of intracellular BLIMP-1 staining per subset is shown in blue histograms (naive controls in red). **(C)** Percentage of each ASC subset and naive B cells (N) expressing IgG, IgA, or IgM isotypes after peak vaccination. **(D)** Quantification of each blood ASC subset (pops 1 to 5) in cells/ml (top) and percentage of PBMCs (bottom). **(E)** Quantitative RNA expression of 5,000 sorted ASC subsets and naive and memory B cells for Pax5 (top), BLIMP-1 (middle), and Xbp-1 (lower), normalized to GAPDH in blood. Relative mRNA expression is expressed in arbitrary units.

**Table 1. Phenotype of blood ASC subsets 1 to 5 (number, %)**

Subsets	CD20 <sup>+</sup>	Surface Ig	CD27 <sup>+</sup>	CD27 <sup>hi</sup>	CD27 <sup>lo</sup>	HLA-DR <sup>+</sup>	Ki-67 <sup>+</sup>	CXCR4 <sup>+</sup>	CD28 <sup>+</sup>	IL-6R <sup>+</sup>	FCGR2B	Mean (cells/ml)	Mean (% MNCs)
Blood	N = 6	N = 3	N = 7	N = 7	N = 5	N = 6	N = 3	N = 4	N = 4	N = 4	N = 3	N = 9	N = 9
1	45 (20-73)	75 (67-87)	31 (14-44)	16 (9-26)	76 (45-92)	67 (42-84)	63 (51-73)	0.5 (0.2-1)	28 (22-38)	28 (20.9-40)	28	1,085 (140-4,107)	0.06 (0.01-0.2)
2	3 (1.7-5)	45 (37-59)	22 (9-49)	71 (46-90)	83 (68-94)	93 (83-99)	33 (27-42)	0.7 (0.1-1.3)	68 (55-79)	18 (3.7-47)	18	3,000 (154-12,186)	0.19 (0.01-0.73)
3	1.5 (0-4)	38 (33-41)	11 (1-33)	89 (67-97)	86 (76-96)	96 (87-100)	33 (25-39)	0.5 (0-1)	77 (59-88)	12 (3.5-29)	12	3,096 (209-19,082)	0.19 (0.01-1.15)
4	1.5 (0-5)	8 (3-11)	18 (3-45)	42 (12-68)	49 (30-67)	65 (40-95)	17 (15-20)	1 (0-3)	32 (23-40)	7 (1.5-16)	7	161 (22-347)	0.011 (0.001-0.026)
5	2 (0-8)	34 (22-50)	14 (0-34)	85 (64-100)	75 (56-93)	98 (90-100)	9 (0-18)	0.1 (0-0.3)	68 (45-86)	25 (1.8-67)	25	199 (16-745)	0.014 (0.001-0.045)

MNCs, mononuclear cells. Ranges for all mean values are shown in parentheses.

*Morphology and expression of PC transcription factors.* The nature of the ASC subsets identified by flow cytometry was validated by multiple approaches including morphology, expression of transcription factors involved in PC differentiation (BLIMP-1 and Xbp-1), and spontaneous antibody secretion. Morphology was ascertained by cytospin with Wright-Giemsa staining of each sorted ASC subset present in the blood after tetanus vaccination of 2 subjects (ages 50 and 59 years). Pops 1 to 5 had ASC characteristics including large size with big, eccentric nuclei and enlarged cytoplasm, distinct nucleoli, and a prominent Golgi zone (Figure 1B). Nearly all cells in pops 2 to 5 had intracellular BLIMP-1 protein detected by flow cytometry (Figure 1B). Interestingly, IgG isotypes were highest in ASC pops 2 to 5 except for pop 1 (Figure 1C). None were observed in naive B cells. Pop 1 had variable expression of BLIMP-1, suggesting it comprises an early or mixed population of ASCs. Pops 2 and 3 (CD19<sup>+</sup> subsets) made up the largest frequencies of all the blood ASC subsets, and pops 4 and 5 (CD19<sup>-</sup> subsets) were the least abundant (Figure 1D). Additionally, pop 4 was quite heterogeneous; thus, additional backgating of the BLIMP-1-positive pop 4 cells showed no difference in forward or side scatter compared to other ASC populations (Supplemental Figure 2).

All peripheral blood ASC populations (pops 1 to 5) were characterized by RNA expression of BLIMP-1 and Xbp-1 and absence of Pax5 (Figure 1E). In contrast, Pax5 expression was higher in naive versus memory B cells, neither of which expressed Xbp-1. BLIMP-1 was undetectable in memory B cells. The lack of Pax5 expression and increased BLIMP-1 expression in pop 1 suggests a process of differentiation from a B cell into an ASC. Xbp-1 is downstream of BLIMP-1 expression; thus, lower Xbp-1 expression observed in pop 1 compared with pops 2 to 5 also suggests that pop 1 may represent an earlier stage in ASC differentiation, or a mixed population of activated B cells that have already downregulated Pax5. A low level of BLIMP-1 expression was observed in naive B cells, which may have been due to a fraction of activated naive cells, or a small number of contaminating B1 cells, since only IgD and CD27 were used to discriminate the naive population, noting that a low level of BLIMP-1 expression has been reported in mouse B1 cells (29).

*Flow characteristics of blood ASC subsets.* As B cells differentiate into ASCs, they undergo massive proliferation and lose features of B cells (such as CD20 and surface Ig), exit cell cycle, gain expression of BLIMP-1, and upregulate receptors for homing to the BM (30-32). Accordingly, we used multiparameter flow cytometry to evaluate these characteristics (Figure 2 and Table 1). As shown in Figure 2A, CD20 was downregulated on nearly every cell in pops 2 to 5, consistent with the loss of CD20 that begins as early as 7 days after vaccination in newly formed ASCs (4). However, pop 1 contained a mixture of cells positive for CD20, suggesting it is the earliest ASC phenotype with downregulation of Pax5 (Figure 1D). In contrast, surface Ig was highest on pop 1 and gradually downregulated in pops 2, 3, and 5 (~34%-45%; only ~8% in pop 4). These proportions of blood ASCs with surface Ig were higher than those found on LLPC (pop D) BM subsets (1). Interestingly, circulating ASC pops 2, 3, and 5 uniformly expressed high levels of CD27, a member of the tumor necrosis factor receptor (TNFR) family that is upregulated during B cell activation and is linked to PC differentiation (33), whereas the lowest frequencies of CD27 expression were found in pop 1 (~17%) (Figure 2A).

HLA-DR, a marker of cell activation previously shown to decrease during PC maturation (9), was highly expressed on nearly all blood ASC

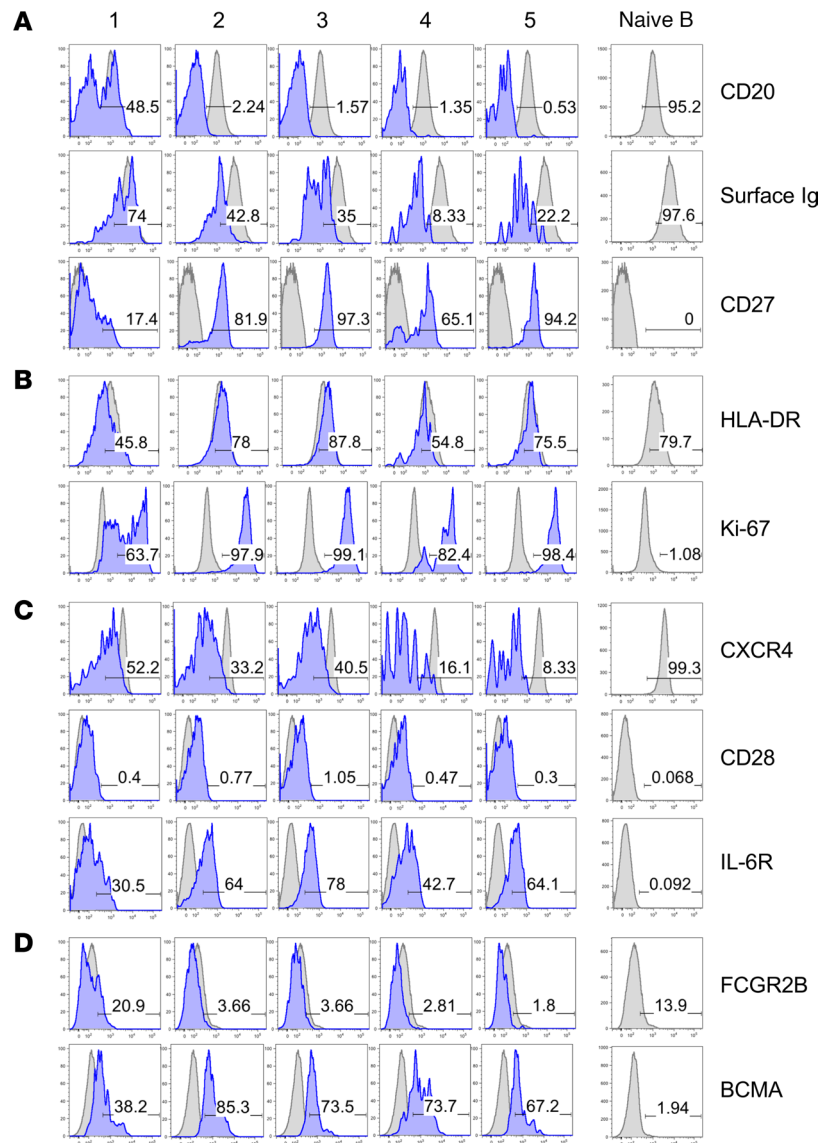


**Figure 2. Phenotype of blood ASC subsets on day 7 after vaccination.** (A) CD20, surface Ig (kappa and lamda), and CD27 staining for blood ASC subsets and naive B cells (CD19<sup>+</sup>IgD<sup>+</sup>CD27<sup>-</sup>) illustrated in blue relative to controls in gray (also shown in right-hand panel). (B) HLA-DR and Ki-67 staining for blood ASC subsets. Far right: CD14<sup>+</sup> peripheral blood monocytes served as controls for HLA-DR staining and naive B cells for Ki-67. (C and D) Frequency of CXCR4, CD28, IL-6R, FCGR2B, and BCMA in blood ASC subsets (pops 2 to 5) and naive B cells. Respective numbers of subjects are listed in Table 1.

subsets (Figure 2B), which contrasts with its near absence on LLPC BM PC subsets (1, 2). We also found that Ki-67, a nuclear protein associated with recent cell division, was expressed by most cells in pops 2 to 5 and at a lower frequency of cells in pop 1 (Figure 2B). Thus, nearly all postvaccination ASCs in peripheral blood expressed Ki-67, consistent with the idea that these cells were recently generated, again in direct contrast to BM PCs (1).

The relative expression of molecules involved in LLPC homing and survival were evaluated on blood ASCs (Figure 2C). For example, CXCR4, a chemokine receptor implicated in PC homing and retention in the BM (32, 34), was most commonly expressed in pop 1 and gradually decreased proportionately in pops 2 through 5 (Figure 2C). CD28, a costimulatory molecule associated with LLPC survival (35), which was known to have approximately 20% expression on BM LLPCs (1), was virtually absent on any of the blood ASC subsets. We previously reported that the IL-6R expression was very low on BM PC subsets despite the important role of IL-6 in PC survival (36). However, in the blood, ASC pops 3 to 5 expressed high levels of

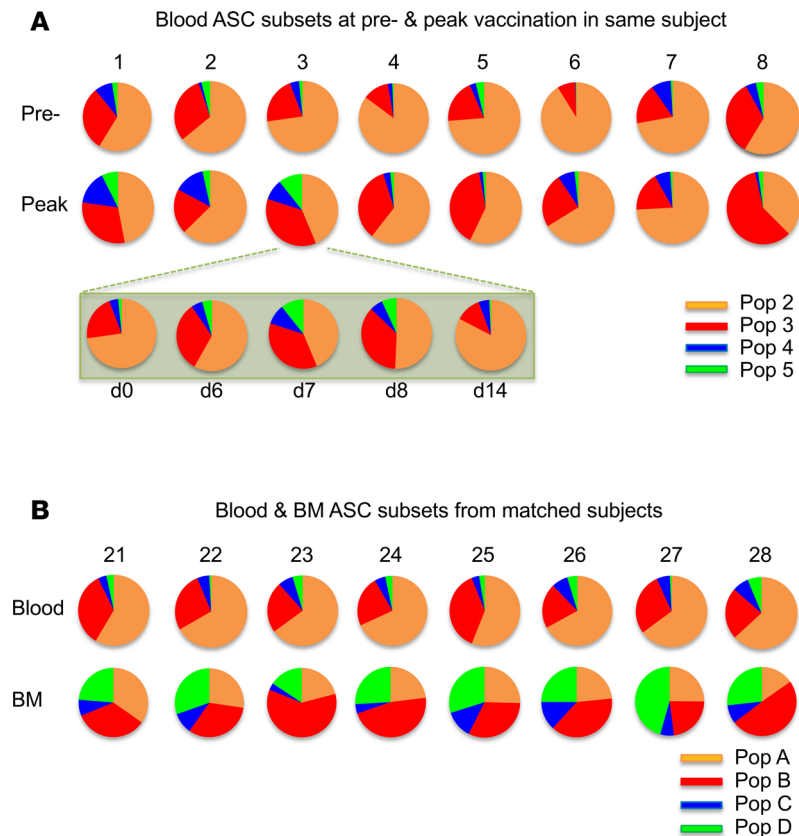


**Figure 3. Ratios of ASC subsets in blood and BM.** (A) Pie charts representing proportions of pops 2, 3, 4, and 5 in the blood from 8 different adult subjects at steady state (top) and at peak (days 6–7) ASC response in blood after tetanus vaccination. The proportion of each ASC subset is represented by the corresponding sector size of the pie chart. Kinetics of the ratios of the ASC in the blood after tetanus vaccination is shown for subject 3 (inset). (B) From 8 additional subjects, ratios of pops A, B, C, and D in the BM and blood pops 2, 3, 4, and 5 were matched at the time of the BM aspirate. ASC subsets in blood and BM (pops 1 and Z) are not included. Pops 2 and A, pops 3 and B, pops 4 and C, and pops 5 and D (LLPC subset) are shown in tan, red, blue, and green, respectively.

IL-6R (Figure 2C). Finally, the expression of the inhibitory FCGR2B, which promotes PC apoptosis (37), showed wide variation from subject to subject, but was typically low in blood ASC subsets compared with BM subsets (1) (Figure 2D). Lastly, B cell maturation antigen (BCMA), also known as TNFR superfamily member 17 (TNFRSF17), the receptor for APRIL, was uniformly expressed on pops 2–5 (Figure 2D), demonstrating the importance of this cytokine. Together, these results demonstrate that blood ASC subsets are Ki-67<sup>+</sup> and HLA-DR<sup>+</sup>, suggestive of recent proliferation and activation.

*ASC subsets before and after vaccination in blood.* Overall, compared with day 0 (~0.5%), we found that ASCs represented a larger fraction of circulating PBMCs 7 days after vaccination but with variable input from the different populations, as CD19<sup>+</sup> (pops 1, 2, and 3) contributed in excess of 95%. This frequency is in keeping with the postvaccination levels of circulating ASCs previously established by enzyme-linked immunospot (ELISpot) analysis, which typically represent a 5- to 20-fold increase over steady-state levels (28). Therefore, we sought to determine the relative contributions of the different ASC subsets to this substantial increase after tetanus vaccination. We performed multicolor flow cytometry in 8 healthy adults prior to (i.e., steady state) and at peak vaccine responses. We removed pop 1 due to its low abundance and heterogeneity. The average total number of ASCs in each population increased after vaccination as follows: pop 2 increased by 7.6-fold, pop 3 increased 33-fold, and pop 5 increased by 13-fold. Thus, the relative abundance at steady-state and peak vaccine responses were different. During steady state, pop 2 (~60%–80%) dominated the ASC ratios with almost no pop 5; however, vaccination induced relative increases of expansions of pops 3, 4, and 5 in all 8 subjects, with corresponding decreases in pop 2 proportionally (Figure 3A). This appearance of CD19<sup>+</sup>CD138<sup>+</sup> fractions (pop 3) for healthy adults after immunization is consistent with previous observations after tetanus vaccination (13).

*Frequencies of ASC subsets in blood and BM.* Direct comparison of the quality and quantity of the ASC subsets in 8 healthy asymptomatic adults (mean age 48.5, range 43 to 56 years) was also performed for matched blood and BM samples from the same subject. Pop A in the BM, which contains surface markers similar to those in ASC pop 2 in the blood, make up a markedly smaller percentage of BM ASC subsets compared with the blood (Figure 3B). The relative frequencies of the different ASCs were remarkably conserved in all 8 BM samples analyzed, with CD138<sup>+</sup> (pops B and D) representing the most abundant subsets. Pop 5 could be detected in the blood in some subjects at steady state, but most of these cells were positive by Ki-67 staining (Figure 2B), thereby distinguishing them from BM pop D (Ki-67<sup>-</sup>) with the same surface markers (1). We found that at steady state, pop 5 had similar Ki-67<sup>+</sup> staining that resembled the blood pop 5 during acute immune responses, implying that they are newly generated ASCs and not BM emigrants released in the blood from the BM niches.

*NGS of the V<sub>H</sub> antibody repertoire of ASC subsets.* NGS was used to assess the complexity and connectivity of the antibody repertoire expressed by the different ASC subsets. Pops 1 to 5 were sorted from a 45-year-old adult after tetanus vaccination and 3,174; 5,000; 5,669; 2,550; and 1,994 cells, respectively, were collected. NGS was performed using Illumina MiSeq Amplicon sequencing with primers positioned in the framework region FR1 of the V<sub>H</sub>1–V<sub>H</sub>6 families, and in constant regions corresponding to the IgM, IgG, and IgA isotypes (Figure 4). Sequences were considered part of the same clonal lineage if they shared the same V and J gene segment rearrangement and a CDR3-H of identical length with at least 85% sequence similarity based on our previous studies (38). Total numbers of lineages for pops 1–5 were 984, 943, 825, 83, and 311, respectively. The overall degree of clonality was quantified using D50 or D20 scores calculated as the number of clonotypes accounting for the top 50% or 20%, respectively, of all size-ranked clones within a given population. For ASC pops 1 to 5 and memory B cells, the IgG D20 scores were 14, 2, 2, 1, 2, and 2, and D50 scores were 65, 4, 6, 3, 5, and 9, respectively, demonstrating that each subset at the peak of the vaccine response is dominated by a small number of substantially expanded ASC clones (Figure 4A). Switched memory (SWM) B cells were also oligoclonal, whereas the naive B cells were polyclonal with D20 and D50 scores of 910 and 3,674, respectively. The diversity of the V<sub>H</sub>-gene repertoire is demonstrated by the Hill diversity score and was highest in pop 1 compared with the other ASC subsets (Figure 4B). Finally, the composition of the isotypes of the V<sub>H</sub> sequences in the ASC subsets (Figure 4C) were switched between IgG and IgA sequences, with predominantly IgA compared with IgG in pop 1, whereas pops 2 to 5 and SWM B cells were higher in IgG. Very little IgM isotypes were found in the ASC subsets or SWM B cells, whereas naive B cells contained only IgM sequences, as expected.

Next, the actively expanded blood IgG, IgA, and IgM ASCs in response to immunization shared similar repertoires, as shown in the outer circo plot tracks (Figure 4D). Connectivity of the repertoires among subsets is also shown by the circo plot (39) (Figure 4D). Blood ASCs were largely oligoclonal with a repertoire dominated by a few clonotypes, many of which in ASC pops 2 to 5 were shared (Figures 4, D and E). The SWM B cells were also highly oligoclonal with many shared clones, in contrast to the naive B cell subset. Many of these same clones were also shared by ASCs in pop 1, but consisted of much smaller clonal populations (Figure 4E). Pops 1 to 5, as well as SWM B cells, were all highly interconnected as quantified by the high Morisita overlap indices (Figure 4F), but this was not the case comparing ASCs with naive B cells. In conclusion, the V<sub>H</sub> repertoire analysis demonstrates oligoclonality, rich interconnections, and predominately IgG isotypes among the circulating ASC subsets and SWM B cells on day 7.

*Mutation analysis and V<sub>H</sub> lineage analyses.* On average, all blood ASC pops 1 to 5, which were mostly class switched to IgG or IgA, were highly mutated with similar average mutation frequency, as defined by the number of mutations in each sequence divided by length of that sequence (Supplemental Figure 3A). Intraclonal mutation analysis was also conducted to determine progression of ASC populations within individual clones. In this analysis, average mutation frequencies for each individual population were compared to average mutation frequencies of all populations in that same clone. By examining the mutation frequencies this way, we can get a better picture of which populations tend to have higher or lower mutation frequencies compared with other populations within the same clone. This analysis showed some deviations of the individual ASC populations' mutation frequencies, namely that pop 4 tended to have the highest mutation frequencies in clones, while SWM and pop 2 tended to have the lowest (Supplemental Figure 3B). To follow the possibility of sequential acquisition of mutations for the different subsets, we analyzed the V<sub>H</sub> repertoire of 5 of the largest individual clones that shared lineages in pops 1 to 5 using IgTree (40) and PHYLIP phylogenetic analysis. Within the 5 clones, the

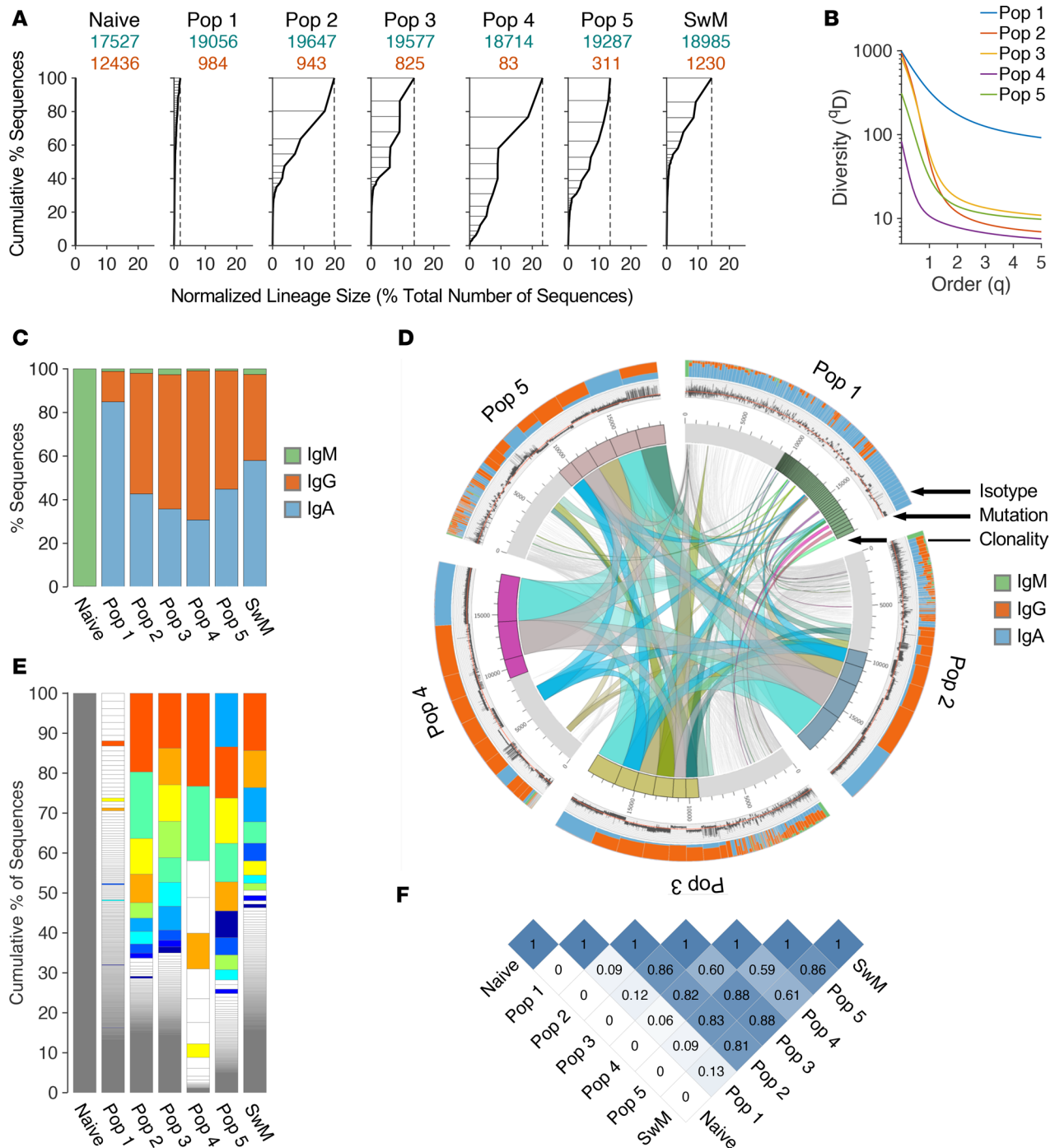


**Figure 4. Next-generation sequencing (NGS) repertoire sequencing of blood ASC subsets.** NGS was used to analyze the clonal repertoire of the ASC populations, naive B cells, and isotype-switched memory B cells. **(A)** Diversity of the repertoire is shown by plotting lineage (clone) size versus the cumulative percentage of sequences determined from size-ranked clones. Largest clones are found at the top of the plot and account for a greater area within the subdivided plots. More diverse repertoires, such as the naive population here, only contain small clones in a more even representation. **(B)** Hill diversity profiles for each population (with different levels of sampling) demonstrate the overall diversity of the repertoire in each of the ASC populations. **(C)** Relative quantities of IgM, IgG, and IgA sequences in each subset. Naive is predominantly IgM. Blood ASC subsets 1 to 5 and switched memory B cells show mostly IgG and IgA. **(D)** Circos plot shows interconnectiveness of the ASC populations by plotting the sequences from each population in clonal size-ranked order, with the largest clones being in the most clockwise portion of each population segment. The outer-most track shows the isotype makeup of each clone by color. The next track in shows mutation frequency of each sequence, with more mutations represented as more distal from the center of the plot. The next track in shows the number of sequences, followed by the clonality displayed by a circular stacked bar plot. Here, only the largest 50% of the clones are colored to avoid blurring of small clones. The internal connections show clones found in multiple populations. **(E)** Stacked bar plots again demonstrate the diversity of the repertoire by showing size-ranked clones as segments taking up a percentage of the total repertoire. The largest 10 clones of all populations are colored and like-colors demonstrate the same clone in multiple populations. **(F)** The Morisita overlap index demonstrates the similarity of repertoires in various populations as a value from 0 (no similarity) to 1 (identical repertoires). The color strength is indicative of interconnectivity.

number of nodes shared among the various populations of ASCs was striking. No apparent progression or sequential differentiation was found, but instead the ASC populations were highly intermixed throughout the phylogenetic tree. An example of one clone shows a deep IgTree structure with high interconnectedness between populations, illustrating the single origin of the multiple blood ASC subsets (Supplemental Figure 3C). Thus, we concluded that sequential increases in progressive accumulation of mutation did not occur from pops 1, 2, 3, 4, and 5, but each clone segregated into independent branches, demonstrating that both CD19<sup>+</sup> and CD19<sup>-</sup> subsets arise from a common B cell progenitor.

*Tetanus IgG secretion in blood ASC subsets.* The secretory function of different ASC subsets was validated by measurement of constitutive antibody secretion as well as participation in antigen-specific responses after tetanus vaccination. Spontaneous total IgG and tetanus-specific IgG without in vitro stimulation were assessed by ELISpot assays in 6 adults (mean age 44 ± 11 years, range 27–59 years) from blood after tetanus boosting. Cells constitutively secreting IgG were detected in all 5 ASC subsets but not every subject had adequate numbers of pops 4 and 5 for FACS analysis. Nonetheless, tetanus-specific IgG ASCs were highly enriched in both CD19<sup>+</sup> (pops 1, 2, and 3) and CD19<sup>-</sup> (pops 4 and 5) ASC fractions when present (mean 19%, 29%, 33%, 33%, and 25% for pops 1 to 5, respectively) (Figure 5, A and B). Thus, all circulating ASCs (including the CD19<sup>-</sup> and CD138<sup>+</sup> subsets) can contribute similarly to the short-term response to tetanus immunization.

*Comparative transcriptome analysis of 3 ASC subsets.* The transcriptomes of pops 2, 3, and 5 were contrasted by analysis of variance of RNA sequencing (RNA-seq) profiles of 6 donors (labeled Sub 06 to 11). Two-way hierarchical clustering of 674 genes differentially expressed among the 3 ASC pops shows that pop 5 is significantly different from pops 2 and 3 (Figure 6A). This basic distinction between the CD19<sup>-</sup> and CD19<sup>+</sup> ASCs is supported by principal component analysis (PCA), since PC1, which captures 56% of the gene expression variance, separates pops 2 and 3 from pop 5, while PC2 (7%) distinguishes pop 2 and pop 3 (Supplemental Figure 4). Furthermore, the 464 genes upregulated in both pops 2 and 3, and 210 genes downregulated relative to pop 5, lead to coclustering of the pairs of samples within individuals, implying that the 2 subtypes are transcriptionally closely related within subjects.

Gene set enrichment analysis (GSEA) reinforces this similarity between pops 2 and 3 in comparison with pop 5 and highlights 29 gene sets that are differentially regulated. These gene sets summarize biological functions that are likely to differ between the pops, and are visualized in 3 different ways since raw summary statistics can misrepresent the relationship between upregulation of transcription and pathway activity. In Figure 6B (and Supplemental Figure 5), the first principal component, which in all cases explains over 45% of the variance in the gene set and has been polarized to ensure that positive values represent a preponderance of upregulated transcripts in the gene set, suggests upregulated pathways of cellular metabolism (adipogenesis, glycolysis, oxidative phosphorylation, fatty acid metabolism, and mTORC1 signaling), stress-induced pathways (DNA repair, UV response, and unfolded protein response), and cell cycle pathways (E2F targets, Myc targets, and G2M checkpoints) in pops 2 and 3. By contrast, several signaling pathways (JAK-STAT3, PI3K-AKT, IFN response, TGF- $\beta$  signaling, and TNF- $\alpha$  signaling) as well as the hypoxic response appear to be elevated in pop 5. Figure 6C reinforces most of these conclusions by presenting the results of normalized enrichment scores for each pathway, but further reveals a gradient whereby pop 2 is more extreme than pop 3 for several pathways, namely downregulation of TNF- $\alpha$  signaling and upregulation of Myc and E2F target. G2M checkpoint regulators decreased expression with acquisition of CD138 and loss of CD19. This difference in dysregulated pathways suggests different cellular functions for pops 2 and 3 in comparison with pop 5.

To visualize differentially expressed genes contributing to pathways, we used spider plots (Figure 7) to contrast the directions of all genes in a gene set whose transcript abundance significantly differed between 2 or more of the ASC subsets. We included some gene sets from which the hallmark pathways are derived and which were of a priori interest. For example, for apoptosis (contained within allograft rejection), hypoxia, TNF- $\alpha$  signaling, and the cell cycle (E2F targets, G2M checkpoints), pop 5 shows very clear upregulation of specific genes resulting in a green polygon that is more expanded along the arcs of the web, whereas the blue-colored pop 3 and pop 2 differential expression is more similar to one another, producing overlapping polygons. This analysis also indicates reduction in expression of all or most of the indicated genes encoding extracellular matrix (ECM) or unfolded protein response (UPR) functions in pop 5. It is not, however, simple to extrapolate transcript abundance to biological functions. For example, the hypoxic response engages 6 genes involved in autophagy; 3 inhibitors of the process (*LDHA*, *PRKCB*, and *CYBB*) are elevated in pop 2,

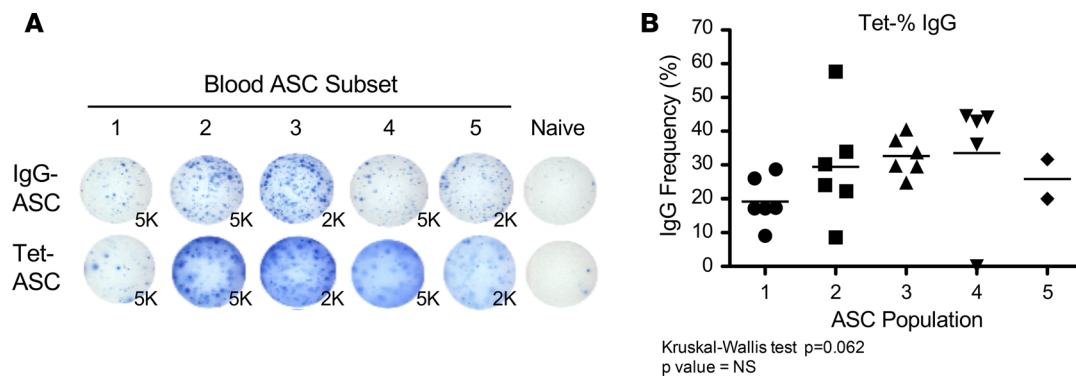


**Figure 5. Vaccine-specific IgG ASC frequencies 7 days after tetanus vaccination. (A)** ELISpot of total IgG (top) and tetanus-specific IgG (lower) ASC frequencies from sorted ASC subsets (pops 1 to 5) in the blood. Naive B cells and total PBMCs are also shown. The total number of sorted cells per well is indicated adjacent to each well. **(B)** Percentage of tetanus-specific IgG/total IgG ASC frequencies from sorted ASC subsets (pops 1–5) in blood ASC populations from 8 adults. Note: some patients had limited frequencies of pops 4 and 5, which could not be sorted.

whereas another, *MAPK3*, is elevated in pop 5, while *PIK3CD* and *MTOR* also regulate ER stress and autophagy, yet are expressed in opposite directions. Prediction of the consequences of differential expression awaits systems modeling that is sensitive to the precise nature of which genes are up- or downregulated jointly.

*ASC survival potential in a human in vitro BM culture system.* To discriminate the differential survival potential upon arrival in the BM microniche, we developed an in vitro cell-free culture system that mimics the human BM microenvironment, as previously described (24). For proof of concept using one abundant blood ASC pop 3, we performed long-term cultures and compared survival for 50 days in the BM MSC secretome alone or secretome with the addition of exogenous APRIL in normoxic or hypoxic conditions from a patient (age 23 years) 7 days after hepatitis A vaccination (Figure 8A). Pop 3 survival was barely maintained by day 50 in the secretome alone in normoxia, but a fraction of cells had better survival in secretome and hypoxia. Interestingly, survival was best overall with the secretome with the addition of exogenous APRIL in hypoxic conditions (Figure 8B). With optimal conditions for ASC survival similar to conditions previously shown with total blood ASCs (24), we sorted ASC pops 2, 3, and 5 from 2 subjects (38 and 25 years old) after tetanus toxoid or influenza vaccination, and cultured them in secretome with the addition of exogenous APRIL in hypoxia for 21 or 48 days, respectively (Figures 8, C and D). The low abundance and heterogeneity of pop 4 made them difficult to culture and maintain. The ASC subsets (pops 2, 3, and 5) were easily sustained in culture and pop 2 may have had a slight survival advantage earlier in culture (days 14–21); however, by day 48, pops 2, 3, and 5 had similar survival rates. Thus, both CD19<sup>+</sup> (pops 2 and 3) and CD19<sup>-</sup> (pop 5) ASC subsets could be maintained in culture for nearly 2 months and all subsets have similar fractions of cells with LLPC potential.

To understand if the ASC maturation required CD138 upregulation, we cultured FACS-isolated CD19<sup>+</sup>CD27<sup>hi</sup>CD38<sup>hi</sup> ASCs from a healthy adult in our BM mimic (MSC secretome, exogenous APRIL, and hypoxic conditions). We performed confocal staining of the ASCs before and 14 days after culture. We show an increased frequency of ASCs with CD138<sup>+</sup> staining on day 14 (Supplemental Figure 6). Whether CD138<sup>-</sup> ASCs upregulated CD138 or CD138<sup>+</sup> ASCs preferentially survived in the cultures will need additional studies. Nonetheless, increased frequencies of CD138<sup>+</sup> ASCs are shown after culture in the BM microniche and are likely related to enhanced survival.

## Discussion

LLPCs are the cornerstone of vaccinology and lifetime protective mediators of infection. It is widely accepted that during acute-recall immune responses, newly generated, proliferative ASCs with a short lifespan produce a transient burst of antigen-specific antibodies. After the initial response decays, pathogen-specific antibody production is sustained at lower levels by mature, nonproliferating, terminally differentiated PCs capable of surviving for many years in the BM (i.e., LLPCs) in the absence of additional antigenic stimulation. Whether all peripheral blood ASCs eventually evolve into LLPCs upon taking residence in BM survival niches, or if short-lived ASC and LLPC precursors are imprinted with a long lifespan based on

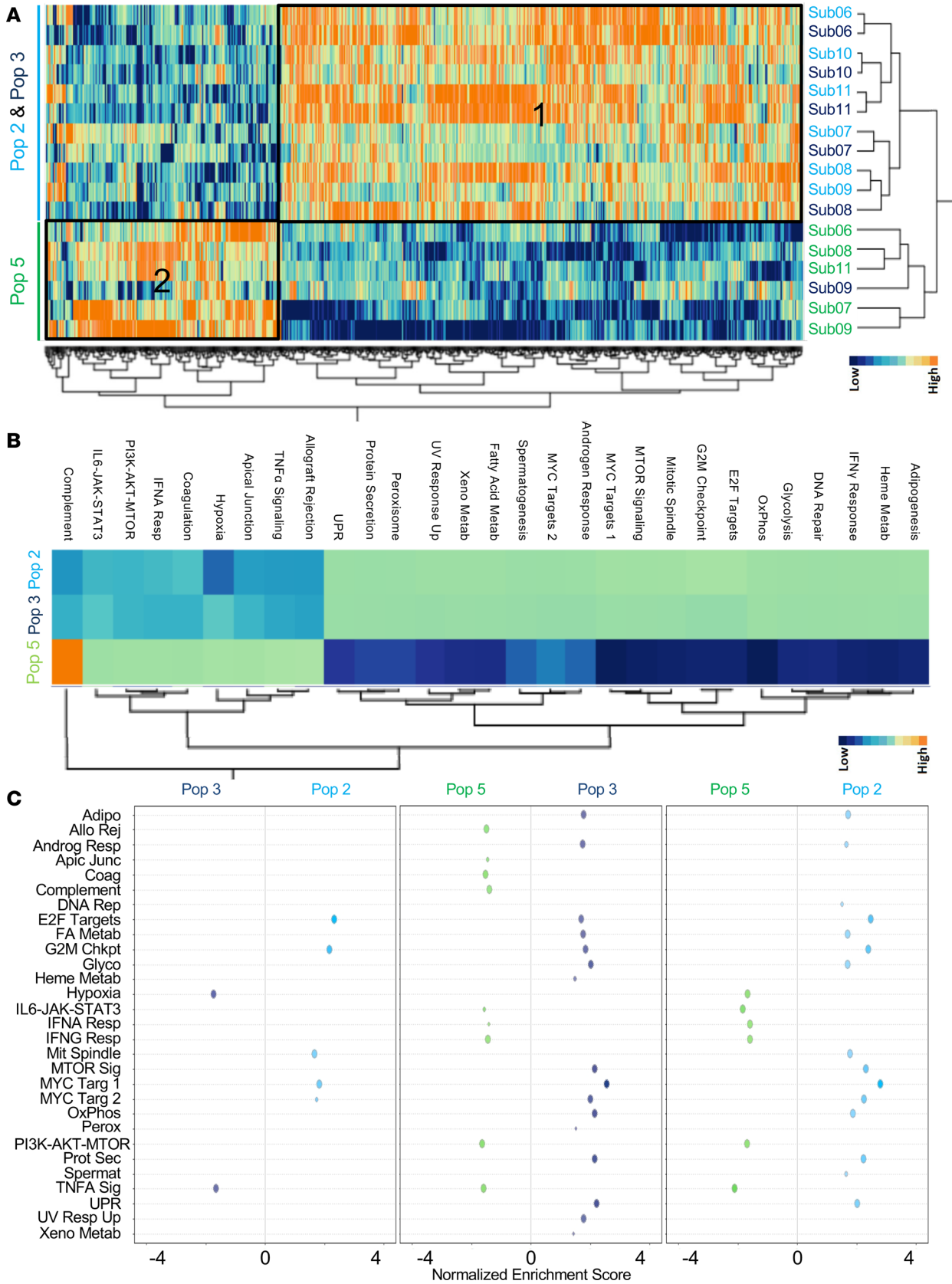


**Figure 6. Transcriptomic analysis of ASC subsets.** (A) Heatmap of 672 transcripts differentially expressed among pop 2, pop 3, and pop 5 RNA-seq profiles from 6 subjects. Red color indicates relatively high expression, blue low expression. Two major blocks of genes upregulated or downregulated in pop 5 relative to pops 2 and 3 are indicated. Sample identities to the right show that pairs of samples from the same individual tend to cluster together. (B) Heatmap of PC1 of 29 gene sets found to be enriched in the differentially expressed genes also shows differentiation of pop 5 from pops 2 and 3, with only minor differences between the latter two. (C) Bubble plots show significantly biased gene sets in each pairwise comparison, with the size of the bubble proportional to the negative logarithm of the *P* value for the normalized enrichment score indicated along the x axis (see Supplemental Table 2 for full list of pathway names).

the relative strength of antigenic signaling received by the corresponding precursor B cells, represent 2 distinct models (41). Discriminating between these 2 models is dependent on the ability to recognize different subsets of ASCs in the blood and their relationship with BM LLPCs.

In this study, we demonstrate the heterogeneity of blood ASC subsets after vaccination by identifying both CD19<sup>+</sup> and CD19<sup>-</sup> subsets with cell surface markers similar to BM PC subsets, as we have previously shown (1). Our results demonstrate significant heterogeneity of human ASC subsets in the blood after vaccination. These heterogeneous subsets include traditional plasmablasts (CD19<sup>+</sup>CD38<sup>hi</sup>CD27<sup>hi</sup>) and 4 newly defined ASC populations distinguished by their relative expression of the surface markers CD19, CD38, and CD138. Discovery and confirmation using FLOCK analysis (4) was essential to comprehensively identify all antibody-producing cells within these subsets. We also show that all circulating ASC subsets are active participants in recent vaccine/immune responses. Interestingly, peripheral CD19<sup>-</sup>CD138<sup>+</sup> ASCs are universally proliferative (>90% Ki-67<sup>+</sup>) and contain antigen-specific responses with frequencies similar to conventional CD19<sup>+</sup>CD138<sup>-</sup> plasmablasts. Also, these antigen-specific ASCs with mature phenotypes are found in the periphery within a few days of immunization, arising at the same time as CD19<sup>+</sup> ASCs. Most importantly, CD19<sup>-</sup> ASCs cannot be the result of displaced CD19<sup>-</sup> BM LLPCs, since BM LLPCs are almost universally Ki-67 negative (1). This conclusion is further supported by the high frequency of recent vaccine-specific cells and oligoclonality in the blood ASC subsets disclosed by V<sub>H</sub> repertoire studies within CD19<sup>-</sup> subsets. In contrast, V<sub>H</sub> repertoires of the BM PC subsets in healthy adults are highly polyclonal, representing an historical archive of a lifetime of exposures (1). Thus, the CD19<sup>-</sup>CD138<sup>+</sup> ASC subsets in the blood are not displaced LLPCs from the BM microniche, but rather newer clones arising from the ongoing vaccine response.

Composition of the antibody repertoire expressed by ASC and B cell subsets provides important clues regarding the origin, diversification, and selection of the compartments in question. Our results portray global repertoires expressed by multiple blood ASC subsets at the peak of vaccination, whereas previous studies had been limited to the analysis of a small number of randomly sampled single cells or global CD19<sup>+</sup>CD27<sup>hi</sup>CD38<sup>hi</sup> ASCs (instead of heterogeneous ASC subsets) (42, 43). The strong connectivity of the ASC subsets with the memory B cell fractions on day 7 may reflect the activated B cell phenotypes previously described as CD19<sup>+</sup>CD71<sup>+</sup>IgD<sup>-</sup>CD38<sup>lo/int</sup> (43). Consistent with single-cell studies, our global analyses demonstrate that responding ASCs were largely oligoclonal with highly variable rates of somatic hypermutation in the expanded clones, including some with rather low mutational load, a finding suggesting that some ASC clones might derive from recent differentiation of naive B cells. Nevertheless, the majority of expanded ASC clones were shared by all blood ASC populations and SWM B cells irrespective of the degree of mutation, which suggests they all derive from a common ancestral precursor B cell.

Consistently, we also observe that, rather than forming a longitudinal gradient of progressive accumulation of mutation from pops 1 to 5 with shared VDJ clonotypes, individual clones within each ASC subset segregated into independent branches. These results indicate that all the circulating ASC subsets, including those with presumed mature phenotypes as indicated by the absence of CD19 and/or expression of CD138, derive from a common B cell progenitor. Then, they appear to develop through parallel differentiation of proliferating cells that acquire the characteristic cell surface phenotypes and divergent patterns of somatic hypermutation. Thus, ASC surface maturation (CD138 or loss of CD19) is likely independent of somatic hypermutation.

Intriguingly, pop 1 had many IgA isotypes that predominated this subset with some connectivity to pops 2–5 and SWM B cells, albeit the least of all the subsets (Figure 4, A–F). Pop 1 ASCs were also the most diverse compared with the other ASC and SWM B cell subsets, suggesting that some ASCs in this population may originate differently. It is known that at steady state circulating ASCs are mainly IgA ASCs (44) (our unpublished data); however, the specificities remain unknown. Thus, pop 1 may contain both early vaccine-specific IgG ASCs and IgA ASCs from other sites. Whether they are homeostatic IgA ASCs specific to our microbial flora would be important to ascertain, but this will require further studies.

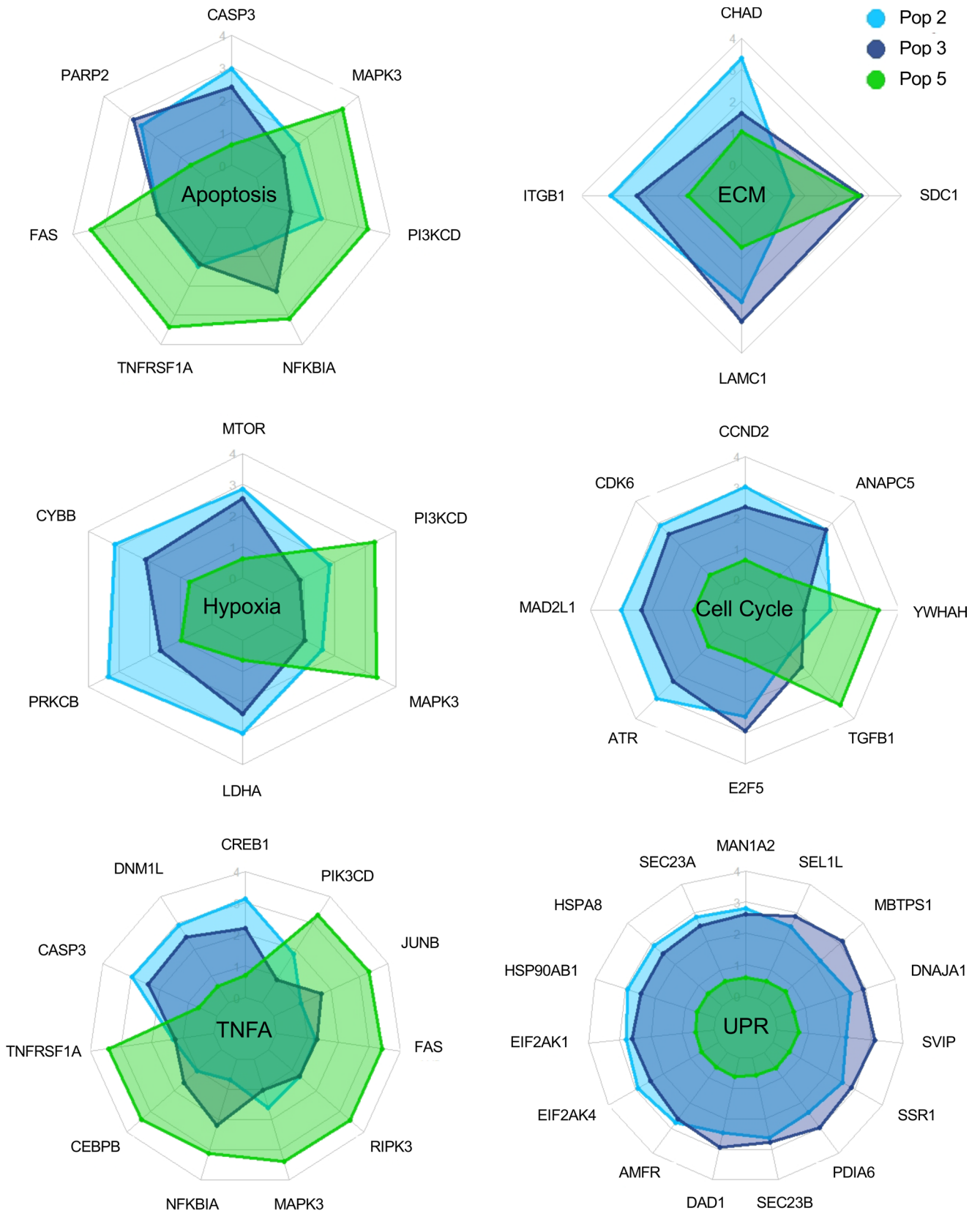


**Figure 7. Significantly differentially expressed genes in selected pathways.** Spider plots of significantly differentially expressed genes in 6 selected pathways showing differences among the 3 ASC populations. Rays of each plot represent transcript abundance for the indicated gene, with low values in the center and high at the periphery. Polygons link observed transcript levels in each cell type, showing how pop 5 differs from pops 2 and 3.

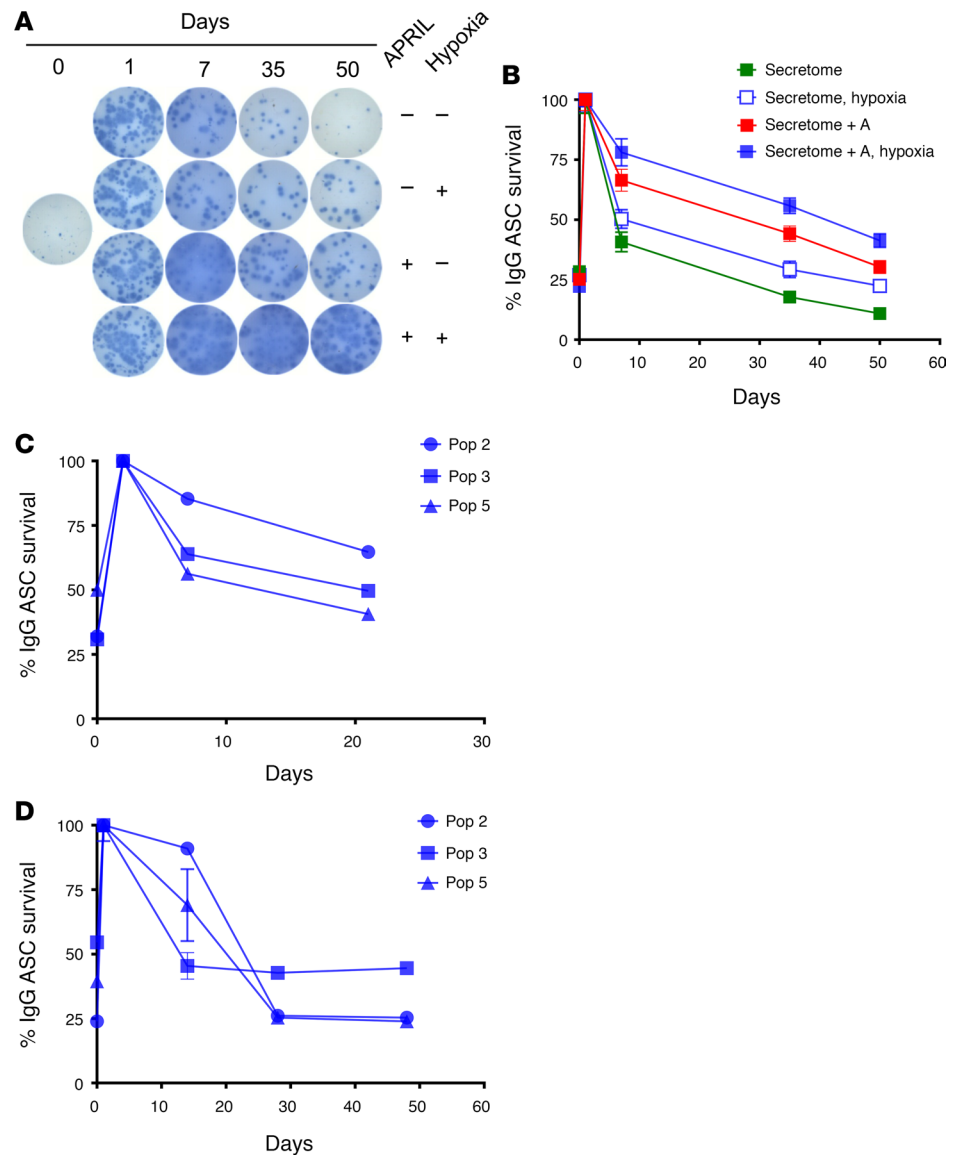


**Figure 8. In vitro human BM microniche systems to measure long-lived survival of the subsets. (A)** IgG ELISpots of pop 3 ASCs from a healthy adult after hepatitis A vaccine on days 0, 7, 35, and 50 in the BM MSC secretome (green) or BM MSC secretome with the addition of exogenous APRIL (red) in normoxia and hypoxia (blue open symbol or blue closed symbol). **(B)** Percentage of IgG ELISpots (relative to the maximal frequency) for pop 3 in MSC secretome in normoxia (green square), MSC secretome in hypoxia (open blue square), MSC secretome with the addition of exogenous APRIL in normoxia (red square), and MSC secretome with the addition of exogenous APRIL in hypoxia (blue square). **(C)** Percentage of IgG ELISpots from pops 2, 3, and 5 (relative to the maximal frequency) from a healthy adult after tetanus vaccination on days 1, 7, and 21 in MSC secretome with the addition of exogenous APRIL in hypoxia. **(D)** Percentage of IgG ELISpots from pops 2, 3, and 5 (relative to the maximal frequency) from a healthy adult after influenza vaccination on days 1, 14, 28, and 48 in MSC secretome with the addition of exogenous APRIL in hypoxia.

Interestingly, pops 2, 3, and 5 had similar survival rates in our cell-free BM microniche system, implying equal survival potential upon arrival in a supportive niche in the body. Other models using in vitro differentiated ASCs had a massive attrition of ASCs in culture since they did not optimize conditions to mimic the human BM microniche that is the naturally occurring site of LLPC survival. Furthermore, they started with B cells that were differentiated to ASCs in vitro (14), compared with our studies that immediately cultured in vivo-differentiated ASCs, which is more physiologically relevant. Lastly, those models used MSC cell lines that are not likely to be as efficient as our validated human in vitro BM microniche system with primary BM MSC secretomes, exogenous cytokines, and hypoxic conditions to maintain human PCs (14, 24).

Mouse models of LLPCs have been described in the BM demonstrating how homing and retention in the BM appears to be a major determinant for the persistence of human LLPCs (25). CXCR4 is important for PC migration and survival in the BM since BM stroma is rich in CXCL12 (45, 46). The CD19<sup>+</sup> blood ASCs expressing higher CXCR4 levels may have potential for homing to supportive BM sites. At the same time, BM-resident LLPCs express very high levels of CXCR4, indicating that CXCL12 may also be involved in BM retention (1). Thus, with proper migration and retention, survival may be guaranteed given transcriptional programs intrinsic to the blood PCs. Since the BM-derived MSCs are an abundant source of CXCL12, whether CXCL12 also has a role in survival or just in retention will need further exploration.

Our models could not discern a survival advantage of ASCs that may have intrinsic properties for BM homing because our system provides the same BM survival microniche equally to each sorted ASC subset (pops 2, 3, and 5). Therefore, the similar survival advantage of all 3 ASC subsets (Figure 8) may in fact reflect equal survival potential but not necessarily equal homing to or retention in the BM microniche.

Recently, CD138, a heparin-sulfate glycoprotein (HSGP), has been shown to potentiate survival of ASCs (16). It was found that the ASCs lacking CD138 were more prone to apoptosis and reduced levels of IL-6 signaling. Evidence of increased ASC expression of surface HSGP is known to be important for the binding of survival factors, such as APRIL, hepatic growth factor (HGF), and epidermal growth factor (EGF), on malignant PCs (47–49); however, it is unclear if it is also important in normal LLPC development. More interestingly, IL-6 and APRIL protect ASCs from apoptosis in experiments using heparin sulfate chains to increase IL-6 and APRIL presentation on the ASC receptors (16). Although both CD138<sup>+</sup> (pops 3 and 5) and CD138<sup>-</sup> (pop 2) ASC subsets had similar survival in our cultures, it was not clear if pop 2 also increased CD138 expression progressively within the *in vitro* BM microniche with higher concentrations of IL-6 and APRIL. These findings imply that the BM environment may play a role in altering the phenotype of an ASC through additional maturation.

CD38<sup>+</sup> ASC maturation appears to involve acquisition of CD138 in pop 3 (CD19<sup>+</sup>CD138<sup>+</sup>) and pop 5 (CD19<sup>-</sup>CD138<sup>+</sup>) cells, suggesting sequential maturation. B cells undergo massive proliferation and then differentiation to become ASCs (50). Our gene expression data indicated engagement of cell cycle, specifically G2M transition, genes among the various subsets, but it remains unclear whether pop 2 is the more proliferative subtype, as would be consistent with a maturation process that starts with pop 2 differentiating into pop 3. Furthermore, pops 2 and 3 showed elevated expression of caspase 3 and so are likely to undergo apoptosis, unless additional ASC maturation is orchestrated. Pop 5 ASCs are quite different from pops 2 and 3, with upregulation of hypoxia, TNF- $\alpha$ , and downregulation of UPR pathways. Because they have downregulated both oxidative phosphorylation and glycolysis, it will be interesting to understand the consequences for their survival, immune-related activity, and potential for ongoing maturation.

Recent work by Neu et al. with single-cell transcriptomes of vaccine- versus non-vaccine-specific ASCs showed that the differences between these 2 subsets were in the glycosylation enzymes (51). These findings are interesting but address very different questions from our work. Our studies depict progression of ASC differentiation to a long-lived phenotype with the comparison of CD19<sup>+</sup> and CD19<sup>-</sup> ASCs with upregulation of pathways such as hypoxia, TNF- $\alpha$ , and UPR involved in LLPC generation, whereas Neu et al. compared vaccine- versus non-vaccine-specific ASCs. Interestingly, the differences between vaccine- and non-vaccine-specific ASCs were relatively minor. One reason could be that similar transcriptomes of vaccine- versus non-vaccine-specific ASCs arise with short-lived (influenza) vaccines. Greater differences may have been observed between vaccine- and non-vaccine-specific ASCs in long-lived immunization such as tetanus. Nonetheless, additional studies are needed to further elucidate mechanisms of early ASCs to understand long-lived vaccine durability.

Whether the local microenvironment is sufficient for LLPC generation is not known. In this study, we show that both CD19<sup>+</sup> and CD19<sup>-</sup> ASCs have similar potential for longevity, suggesting that both extrinsic factors and intrinsic ASC programming may be essential. However, we also tested ASC subsets from vaccines with relatively long-lived protection such as tetanus (10 years), hepatitis A (25 years), and intermediate longevity for influenza vaccines (52, 53). We have not yet evaluated short-lived vaccines to test the imprinting models with differential strength of antigen signal, or costimulation with Tfh cells, to address this question. Hence, we show that the unique BM locale is necessary, but whether it is sufficient is still unclear.

The improved survival in hypoxia within the BM microniche system was quite surprising. Clearly, the circulating ASCs in normoxic peripheral blood must adapt to hostile conditions of 2.5% oxygen. Whether these programs are intrinsic to the blood ASCs as they exit the germinal centers or whether they further

differentiate to acclimatize to these microniches is not known. Moreover, mechanisms of how hypoxia provides a survival advantage will also need systematic evaluation of cultured ASCs.

In conclusion, we find that significant heterogeneity of ASC subsets resides in the blood during active immune responses in healthy adults. Our results demonstrate that the timing of ASC subsets with markers of maturity (loss of CD19 and acquisition of CD138) are concurrent to CD19<sup>+</sup> plasmablasts (CD19<sup>+</sup>CD27<sup>hi</sup>CD38<sup>hi</sup>) in the blood. Furthermore, both CD19<sup>+</sup> and CD19<sup>-</sup> ASC subsets are newly generated, and all are participants of the new vaccine response. On aggregate, our results favor an ongoing evolution of ASCs once released into the peripheral blood and upon arrival to the BM niches. Thus, it is likely that the ASCs have intrinsic mechanisms of maturation (acquisition of CD138 and loss of B cells surface markers, such as CD19), which are further enhanced with extrinsic signals from the BM microniche such as IL-6 and APRIL. The surface surrogate markers may in fact be associated with important inflammatory mediators, such as IL-6, TNF- $\alpha$ , apoptotic pathways, along with metabolic pathway regulation to finally mature into LLPCs. Understanding these mechanisms will be important to study diseases of allergy, transplantation, and autoimmunity and to help develop better long-lived vaccines.

## Methods

**Subjects and study approval.** Vaccinated and healthy asymptomatic adults (102 healthy adult subjects, 22 to 65 years old, mean  $42 \pm 11$  years, 72 female, 30 male) were enrolled in this study at the University of Rochester Medical Center and Emory University during 2008–2017. Subjects received the tetanus toxoid Td or combination Tdap, influenza, or hepatitis A vaccines as a part of routine medical care. PBMCs were isolated before vaccination, and on days 6–7 for all vaccination subjects. All studies were approved by the Institutional Review Boards at the University of Rochester Medical Center and at Emory University. Written informed consent from participants was obtained.

**BM aspirates.** BM aspirates used for isolating ASC subsets were obtained from 8 healthy adults (43 to 56 years old, mean  $49 \pm 5$  years, all female). Mononuclear cells were isolated by density gradient centrifugation. Peripheral blood was also collected from 8 subjects at the time of BM aspiration and PBMCs were isolated. Isolation and expansion of healthy BM-derived MSCs (from 2 unrelated healthy BM donors) and subsequent making of the MSC secretome were performed as previously described (24).

**Multicolor flow cytometry.** PBMCs from peripheral blood or BM were isolated using a Ficoll density gradient and stained with the following anti-human antibody staining reagents: Ki-67–FITC (catalog, MHKI6701), CD3–PE-Cy5.5 (catalog, MHCD0318), CD14–PE-Cy5.5 (catalog, MHCD1418) (Invitrogen); CD20-Cy5 (catalog, 15-0209), CXCR4–PE-Cy5 (catalog, 15-9999), CD27–APC-eFluor 780 (catalog, 47-0279) (eBioscience); CD28-PE (BioLegend, catalog 302907); CD19–PE-Cy7 (catalog, 557835), IgD-PE (catalog, 555779), IL6R-PE (catalog, 561696), kappa- or lambda-PE (kappa, 555792; lambda, 555797), CD38–Pacific Blue (catalog, 561378), HLA-DR–Alexa Fluor 700 (catalog, 560743) (BD Pharmingen); CD138-APC (Miltenyi Biotec, catalog 130-091-250); and FCGR2B–Alexa Fluor 647 (custom conjugated by I. Sanz). The cells were analyzed on an LSRII flow cytometer (BD Biosciences).

**FLOCK analysis.** FLOCK is a web-based program publically available for open use by the immunology research community through the Immunology Database and Analysis Portal—ImmPort (<http://www.immport.org>) (4). FLOCK is a novel multidimensional automated flow gating program that uses a density-based clustering approach to algorithmically identify cell populations from multiple samples in an unbiased fashion, thereby eliminating operator-dependent variability (4). FLOCK analysis was used for both total CD19<sup>+</sup>CD3<sup>-</sup>CD14<sup>-</sup> and CD19<sup>-</sup>CD3<sup>-</sup>CD14<sup>-</sup> PBMC populations from 6 blood samples to identify ASC subsets in an unsupervised fashion. These were subsequently isolated by sorting with cell-type specific antibodies.

**ASC subsets sorted by flow cytometry.** CD3 and CD14 cells were removed by positive selection (CD3 and CD14 positive selection, Miltenyi Biotec; CD3, 130-050-101; CD14, 130-050-201) from the mononuclear cells isolated from blood or BM. CD3<sup>-</sup>CD14<sup>-</sup> cell fractions were stained with the following anti-human antibody staining reagents: IgD-PE (catalog, 555779), CD19–PE-Cy7 (catalog, 557835), CD38–Pacific Blue (catalog, 561378) (BD Pharmingen); CD3–PE-Cy5.5 (catalog MHCD0318), CD14–PE-Cy5.5 (catalog MHCD1418) (Invitrogen); CD138-APC (Miltenyi Biotec, catalog 130-091-250); and CD27–APC-eFluor 780 (eBioscience, catalog 47-0279). Naive and memory B cell fractions as well as multiple ASC subsets were collected (see Figure 1). Approximately 5,000 to 100,000 cells were collected for each population.

**Cytospins of sorted ASC subsets.** Cytospins were performed from sorted ASCs in the blood at 1,300 rpm for 5 minutes on the Cytospin 4 (Thermo Fisher Scientific). Approximately 5,000 sorted cells per subset

were dried overnight on albumin-coated slides and stained with Wright stain. Morphology was reviewed by a board certified pathologist and hematologist.

*In vitro culture systems for ASCs.* In vitro cultures of human blood ASCs were performed as previously described (24). Briefly, ASCs were cultured in cell-free MSC secretome media in 96-well flat-bottom cell culture plates (Corning/Sigma) at 37°C in a humid, 5% CO<sub>2</sub>, 95% air (20% O<sub>2</sub>) incubator or in hypoxic culture conditions (2.5% O<sub>2</sub>) at 37°C in a modular incubator chamber (Billups-Rothenberg) that was infused with a preanalyzed gas mixture (AirGas) or in a cell culture incubator programmed for the desired O<sub>2</sub> tension. The blood ASC survival and function were assessed by ELISpot assays, and their output values were expressed as the percentage of maximal IgG-secreting ASCs, which typically occurred on days 1–3.

*Total Ig and antigen-specific ELISpot assays.* To assess survival and Ig secretion function of cultured ASCs, ELISpot assay was performed, as previously described (5, 6, 24, 28). Briefly, PBMCs, sorted ASCs, or B cell subsets were added to 96-well ELISpot plates coated with anti-human IgG (5 µg/ml, Jackson ImmunoResearch), anti-human IgA (5 µg/ml, Jackson ImmunoResearch), or tetanus toxoid (2 µg/ml, EMD Biosciences), and were incubated overnight. Wells were washed and bound antibodies were detected with alkaline phosphatase-conjugated anti-human IgG antibody (1 µg/ml, Jackson ImmunoResearch), alkaline phosphatase-conjugated anti-human IgA antibody (1 µg/ml, Jackson ImmunoResearch), and developed with a VECTOR Blue Alkaline Phosphatase Substrate Kit III (Vector Laboratories). Spots in each well were counted using the CTL immunospot reader (Cellular Technologies Ltd).

*Quantitative PCR for expression of select transcription factor genes from mRNA.* Five thousand cells were sorted from each population as described above. Total cellular RNA was isolated using the RNeasy Mini Kit (Qiagen) by following the manufacturer's protocol. Approximately 400 pg of RNA was reverse transcribed using the iScript RT Kit (Bio-Rad). Aliquots of the resulting single-stranded cDNA products were included with BLIMP-1, Pax5, or GAPDH TaqMan assays (assay IDs: Hs00153357\_m1, Hs00172003\_m1, Hs00231936\_m1, and Hs02758991\_g1; Life Technologies) using IQ Supermix (Bio-Rad) and amplified using a Bio-Rad CFX96 Real-time PCR Detection System for 50 cycles. Resulting Ct values were normalized to GAPDH levels and relative target mRNA for each population was calculated based on a standard curve created using total RNA from all populations.

*RNA transcriptome analysis.* RNA was isolated from sorted ASC subsets from peripheral blood samples for 6 adult donors. RNA-seq was performed as recommended by the manufacturer (Illumina Iix). Briefly, first-hand cDNA was amplified using random hexamers. Following end repair, addition of adaptor ligation, agarose gel isolation of 200-bp cDNA, and PCR amplification of the 200-bp cDNA, the samples were sequenced on an Illumina HiSeq 2000. Over 25 million single-end sequences were obtained per sample, and aligned to the reference annotated human genome hg38 using STAR (54). Exon-level data for approximately 25,000 known gene sequences per sample were identified and consolidated using HTSeq (55) to yield gene-level expression values, then normalized to total counts per gene per million total aligned reads and subsequently TMM values in edgeR (56) that were converted to the log<sub>2</sub> scale. The RNA-seq data have been deposited in the NCBI's Gene Expression Omnibus database (GSE116971).

Differential expression was assessed with the GLM ANOVA routine in JMP Genomics v8.0 (SAS Institute) after further normalization using the SNM procedure in R to remove batch effects with ASC population as the Biological variable and Batch as the adjustment variable with the Rm = True option (57). A lower threshold of 3 log<sub>2</sub> units for inclusion was selected by plotting the coefficient of variance against average abundance. All analyses were qualitatively confirmed for the raw TMM values without SNM. Gene expression was visualized by hierarchical clustering using standardization of each gene across individuals and Ward's method to weight the correlations in JMP Genomics.

*Pathway analysis.* GSEA was performed using the Broad Institute's preranked hallmark pathway gene lists (58, 59). For each of 29 significantly enriched pathways (FDR < 0.05; Kolmogorov-Smirnov nominal *P* < 0.05), the first principal component of the genes computed in R was used to visualize the overall regulation of the gene set. Because PC1 is somewhat arbitrarily signed, we compared these values with the direction of normalized enrichment and adjusted the sign to be concordant with an abundance of upregulation, contrasting pop 5 with pops 2 and 3. Because PC1 is dominated by strongly coregulated genes, it does not necessarily give the same results or significance values as normalized enrichment based on all of the genes in the pathway. An additional 6 pathways were excluded from further consideration because PC1 explained less than 20% of the variance, indicating little covariance; the 29 highlighted pathways all have PC1 explaining greater than 45% of the variance of the genes. Supplemental Figure 5 provides details for 12 gene sets (Allograft Rejection,

Coagulation, Complement, DNA Repair, Heme Metabolism, IFNG Response, Mitotic Spindle, MTORC1 Signaling, Peroxisome, Spermatogenesis, UV Response Up, and Xenobiotic Metabolism) where there is some discordance between the two modes of analysis. Most cases are because PC1 is computed from both up- and downregulated genes that strongly differ among pops, whereas the enrichment score indicates the significance of bias in direction of expression of all genes in the pathway assessed by a t-statistic of the ranks and evaluated relative to 1,000 random permutations. A more granular representation of specific subsets of 6 of these hallmark gene sets was performed for significantly differentially expressed genes annotated to Apoptosis, Extracellular Matrix, Hypoxia, Cell Cycle, TNFA Signaling, and the Unfolded Protein Response. Since the spider plots only represent a minority of the genes, they do not always give the same direction of effect as obtained with the other 2 methods, but they do portray the differential expression of select key genes.

*V<sub>H</sub>NGS.* Total cellular RNA was isolated from naive B cells, SWM B cells, and pops 1, 2, 3, 4, and 5 from blood after tetanus vaccination using the RNeasy Mini Kit (Qiagen) by following the manufacturer's protocol. Approximately 400 pg of RNA was reverse transcribed using the iScript RT kit (Bio-Rad). Resulting cDNA products were included with 50 nM primers specific for V<sub>H</sub>1–V<sub>H</sub>6 and 250 nM IgA, IgM, and IgG constant region-specific primers in a 25- $\mu$ l PCR reaction using High Fidelity Platinum PCR Supermix (Life Technologies). Nextera indices were added and products were sequenced on an Illumina MiSeq with a depth of approximately 300,000 sequences per sample. Sequences were quality filtered and aligned with IMGT.org/HighVquest (60). Sequences were then analyzed for V-region mutations and clonality using programs developed in house and made previously available for public use (38). All clonal assignments were based on matching V and J regions, matching CDR3 length, and 85% CDR3 homology. MatLab (MathWorks) or Circos tools (39) was used for visualization.

*IgG phylogenetic analysis.* Precursor-product relationships of shared clones from blood B cell subsets and ASC populations were assessed using 2 forms of phylogenetic analysis: IgTree (40) and PHYLIP. Sequences from ASC populations and SWM B cells were used to construct trees. The largest 5 shared clones were selected for IgTree analysis and the top 2 clones were used in PHYLIP analysis for verification.

*Statistics.* The Wilcoxon signed-rank test was used to compare paired IgG and IgA isotype frequencies from each subset, and the Kruskal-Wallis test was used to compare antigen-specific IgG ASC frequencies in the blood or BM ASC subsets, with Dunn's adjustment for multiple comparisons. For the RNA-seq data we assumed a negative binomial distribution and used a generalized linear model (GLM) for analysis of variance (ANOVA). This was followed by specific contrasts between populations in blood and between populations in BM to generate *P* values. All *P* values for gene lists were adjusted for false discovery rate to control for type I error due to multiple hypothesis testing (61).

## Author contributions

SG, DCN, JLH, CT, AFR, and CFF carried out the experiments. RM, CLS, SK, DK, and RHS helped with the experiments. GG supervised the bioinformatics analysis. Yu Qian was instrumental with the FLOCK program for discovery of subsets. IS helped conceive the experimental design. FEHL designed and supervised the experiments and wrote the manuscript.

## Acknowledgments

We thank Deanna Maffett, Jennifer Scantlin, Hinel Patel, Maya Lindsay, Claudine Nkurunziza, Vanessa Engineer, Frances Lee, Fikrea Tesema, and Sang Le for their dedication to human subject recruitment. We thank K.Y. Chiang and E. Waller for their assistance with bone marrows. We thank Chelsea Cook for her assistance in the cytopins and staining. We also thank the Flow Cytometry Cores at University of Rochester Medical Center and Emory University (including R. Karaffa, K. Fife, W. Harris, E. Mahar, and A. Rae) for their assistance. We thank the Atlanta Clinical and Translational Science Institute for their assistance in obtaining bone marrow. This work was supported by NIH/NIAID R01AI121252, K23 AI67501, P01AI125180, U19AI1109962, 5 P01 A1078907-04, R37AI049660, U01AI045969, Autoimmunity Center of Excellence ARRA:AI056390-06S2, HHSN266200500030C (N01-AI50029), AI078907, AI049600, and NIH/NCATS UL1 TR000454.

Address correspondence to: F. Eun-Hyung Lee, Division of Pulmonary, Allergy, Critical Care, and Sleep Medicine, Department of Medicine, Emory University, 615 Michael Street, Suite 205, Atlanta, Georgia 30322, USA. Phone: 404.712.2970; Email: f.e.lee@emory.edu.

- Halliley JL, et al. Long-lived plasma cells are contained within the CD19(-)CD38(hi)CD138(+) subset in human bone marrow. *Immunity*. 2015;43(1):132–145.
- Mei HE, et al. A unique population of IgG-expressing plasma cells lacking CD19 is enriched in human bone marrow. *Blood*. 2015;125(11):1739–1748.
- Landsverk OJ, et al. Antibody-secreting plasma cells persist for decades in human intestine. *J Exp Med*. 2017;214(2):309–317.
- Qian Y, et al. Elucidation of seventeen human peripheral blood B-cell subsets and quantification of the tetanus response using a density-based method for the automated identification of cell populations in multidimensional flow cytometry data. *Cytometry B Clin Cytom*. 2010;78 Suppl 1:S69–S82.
- Lee FE, et al. Circulating human antibody-secreting cells during vaccinations and respiratory viral infections are characterized by high specificity and lack of bystander effect. *J Immunol*. 2011;186(9):5514–5521.
- Halliley JL, et al. Peak frequencies of circulating human influenza-specific antibody secreting cells correlate with serum antibody response after immunization. *Vaccine*. 2010;28(20):3582–3587.
- Moldoveanu Z, Clements ML, Prince SJ, Murphy BR, Mestecky J. Human immune responses to influenza virus vaccines administered by systemic or mucosal routes. *Vaccine*. 1995;13(11):1006–1012.
- Terstappen LW, Johnsen S, Segers-Nolten IM, Loken MR. Identification and characterization of plasma cells in normal human bone marrow by high-resolution flow cytometry. *Blood*. 1990;76(9):1739–1747.
- Medina F, Segundo C, Campos-Caro A, González-García I, Brieva JA. The heterogeneity shown by human plasma cells from tonsil, blood, and bone marrow reveals graded stages of increasing maturity, but local profiles of adhesion molecule expression. *Blood*. 2002;99(6):2154–2161.
- Arce S, et al. CD38 low IgG-secreting cells are precursors of various CD38 high-expressing plasma cell populations. *J Leukoc Biol*. 2004;75(6):1022–1028.
- Hargreaves DC, et al. A coordinated change in chemokine responsiveness guides plasma cell movements. *J Exp Med*. 2001;194(1):45–56.
- Caraux A, et al. Circulating human B and plasma cells. Age-associated changes in counts and detailed characterization of circulating normal CD138<sup>-</sup> and CD138<sup>+</sup> plasma cells. *Haematologica*. 2010;95(6):1016–1020.
- González-García I, Ocaña E, Jiménez-Gómez G, Campos-Caro A, Brieva JA. Immunization-induced perturbation of human blood plasma cell pool: progressive maturation, IL-6 responsiveness, and high PRDI-BF1/BLIMP1 expression are critical distinctions between antigen-specific and nonspecific plasma cells. *J Immunol*. 2006;176(7):4042–4050.
- Arumugakani G, et al. Early emergence of CD19-negative human antibody-secreting cells at the plasmablast to plasma cell transition. *J Immunol*. 2017;198(12):4618–4628.
- Szysko EA, Brun JG, Skarstein K, Peck AB, Jonsson R, Brokstad KA. Phenotypic diversity of peripheral blood plasma cells in primary Sjögren's syndrome. *Scand J Immunol*. 2011;73(1):18–28.
- McCarron MJ, Park PW, Fooksman DR. CD138 mediates selection of mature plasma cells by regulating their survival. *Blood*. 2017;129(20):2749–2759.
- Lam WY, et al. Mitochondrial pyruvate import promotes long-term survival of antibody-secreting plasma cells. *Immunity*. 2016;45(1):60–73.
- Pengo N, et al. Plasma cells require autophagy for sustainable immunoglobulin production. *Nat Immunol*. 2013;14(3):298–305.
- Ozaki K, et al. A critical role for IL-21 in regulating immunoglobulin production. *Science*. 2002;298(5598):1630–1634.
- Rasheed MA, et al. Interleukin-21 is a critical cytokine for the generation of virus-specific long-lived plasma cells. *J Virol*. 2013;87(13):7737–7746.
- Linterman MA, et al. IL-21 acts directly on B cells to regulate Bcl-6 expression and germinal center responses. *J Exp Med*. 2010;207(2):353–363.
- He J, et al. Circulating precursor CCR7(lo)PD-1(hi) CXCR5+ CD4+ T cells indicate Tfh cell activity and promote antibody responses upon antigen reexposure. *Immunity*. 2013;39(4):770–781.
- Tangye SG, Ma CS, Brink R, Deenick EK. The good, the bad and the ugly - TFH cells in human health and disease. *Nat Rev Immunol*. 2013;13(6):412–426.
- Nguyen DC, et al. Factors of the bone marrow microniche that support human plasma cell survival and immunoglobulin secretion. *Nat Commun*. 2018;9(1):3698.
- Odendahl M, et al. Generation of migratory antigen-specific plasma blasts and mobilization of resident plasma cells in a secondary immune response. *Blood*. 2005;105(4):1614–1621.
- González-García I, Rodríguez-Bayona B, Mora-López F, Campos-Caro A, Brieva JA. Increased survival is a selective feature of human circulating antigen-induced plasma cells synthesizing high-affinity antibodies. *Blood*. 2008;111(2):741–749.
- González-García I, Ocaña E, Jiménez-Gómez G, Campos-Caro A, Brieva JA. Immunization-induced perturbation of human blood plasma cell pool: progressive maturation, IL-6 responsiveness, and high PRDI-BF1/BLIMP1 expression are critical distinctions between antigen-specific and nonspecific plasma cells. *J Immunol*. 2006;176(7):4042–4050.
- Kyu SY, et al. Frequencies of human influenza-specific antibody secreting cells or plasmablasts post vaccination from fresh and frozen peripheral blood mononuclear cells. *J Immunol Methods*. 2009;340(1):42–47.
- Fairfax KA, et al. Different kinetics of blimp-1 induction in B cell subsets revealed by reporter gene. *J Immunol*. 2007;178(7):4104–4111.
- Tourigny MR, et al. CDK inhibitor p18(INK4c) is required for the generation of functional plasma cells. *Immunity*. 2002;17(2):179–189.
- Turner CA, Mack DH, Davis MM. Blimp-1, a novel zinc finger-containing protein that can drive the maturation of B lymphocytes into immunoglobulin-secreting cells. *Cell*. 1994;77(2):297–306.
- Hauser AE, et al. Chemotactic responsiveness toward ligands for CXCR3 and CXCR4 is regulated on plasma blasts during the time course of a memory immune response. *J Immunol*. 2002;169(3):1277–1282.
- Avery DT, Ellyard JI, Mackay F, Corcoran LM, Hodgkin PD, Tangye SG. Increased expression of CD27 on activated human memory B cells correlates with their commitment to the plasma cell lineage. *J Immunol*. 2005;174(7):4034–4042.
- Nie Y, Waite J, Brewer F, Sunshine MJ, Littman DR, Zou YR. The role of CXCR4 in maintaining peripheral B cell compartments

- and humoral immunity. *J Exp Med.* 2004;200(9):1145–1156.
35. Rozanski CH, et al. Sustained antibody responses depend on CD28 function in bone marrow-resident plasma cells. *J Exp Med.* 2011;208(7):1435–1446.
36. Hilbert DM, Kopf M, Mock BA, Köhler G, Rudikoff S. Interleukin 6 is essential for in vivo development of B lineage neoplasms. *J Exp Med.* 1995;182(1):243–248.
37. Xiang Z, et al. FcγRIIb controls bone marrow plasma cell persistence and apoptosis. *Nat Immunol.* 2007;8(4):419–429.
38. Tipton CM, et al. Diversity, cellular origin and autoreactivity of antibody-secreting cell population expansions in acute systemic lupus erythematosus. *Nat Immunol.* 2015;16(7):755–765.
39. Krzywinski M, et al. Circos: an information aesthetic for comparative genomics. *Genome Res.* 2009;19(9):1639–1645.
40. Barak M, Zuckerman NS, Edelman H, Unger R, Mehr R. IgTree: creating immunoglobulin variable region gene lineage trees. *J Immunol Methods.* 2008;338(1-2):67–74.
41. Amanna IJ, Slifka MK. Mechanisms that determine plasma cell lifespan and the duration of humoral immunity. *Immunol Rev.* 2010;236:125–138.
42. Wrämmert J, et al. Rapid cloning of high-affinity human monoclonal antibodies against influenza virus. *Nature.* 2008;453(7195):667–671.
43. Ellebedy AH, et al. Defining antigen-specific plasmablast and memory B cell subsets in human blood after viral infection or vaccination. *Nat Immunol.* 2016;17(10):1226–1234.
44. Mei HE, et al. Blood-borne human plasma cells in steady state are derived from mucosal immune responses. *Blood.* 2009;113(11):2461–2469.
45. Tashiro K, Tada H, Heilker R, Shirozu M, Nakano T, Honjo T. Signal sequence trap: a cloning strategy for secreted proteins and type I membrane proteins. *Science.* 1993;261(5121):600–603.
46. Méndez-Ferrer S, Frenette PS. Hematopoietic stem cell trafficking: regulated adhesion and attraction to bone marrow microenvironment. *Ann N Y Acad Sci.* 2007;1116:392–413.
47. Moreaux J, et al. APRIL and TACI interact with syndecan-1 on the surface of multiple myeloma cells to form an essential survival loop. *Eur J Haematol.* 2009;83(2):119–129.
48. Mahtouk K, et al. Heparan sulphate proteoglycans are essential for the myeloma cell growth activity of EGF-family ligands in multiple myeloma. *Oncogene.* 2006;25(54):7180–7191.
49. Derksen PW, et al. The hepatocyte growth factor/Met pathway controls proliferation and apoptosis in multiple myeloma. *Leukemia.* 2003;17(4):764–774.
50. Barwick BG, Schärer CD, Bally APR, Boss JM. Plasma cell differentiation is coupled to division-dependent DNA hypomethylation and gene regulation. *Nat Immunol.* 2016;17(10):1216–1225.
51. Neu KE, et al. Spec-seq unveils transcriptional subpopulations of antibody-secreting cells following influenza vaccination. *J Clin Invest.* 2019;129(1):93–105.
52. Amanna IJ, Carlson NE, Slifka MK. Duration of humoral immunity to common viral and vaccine antigens. *N Engl J Med.* 2007;357(19):1903–1915.
53. Ott JJ, Irving G, Wiersma ST. Long-term protective effects of hepatitis A vaccines. A systematic review. *Vaccine.* 2012;31(1):3–11.
54. Dobin A, et al. STAR: ultrafast universal RNA-seq aligner. *Bioinformatics.* 2013;29(1):15–21.
55. Anders S, Pyl PT, Huber W. HTSeq—a Python framework to work with high-throughput sequencing data. *Bioinformatics.* 2015;31(2):166–169.
56. Robinson MD, McCarthy DJ, Smyth GK. edgeR: a Bioconductor package for differential expression analysis of digital gene expression data. *Bioinformatics.* 2010;26(1):139–140.
57. Mecham BH, Nelson PS, Storey JD. Supervised normalization of microarrays. *Bioinformatics.* 2010;26(10):1308–1315.
58. Subramanian A, et al. Gene set enrichment analysis: a knowledge-based approach for interpreting genome-wide expression profiles. *Proc Natl Acad Sci USA.* 2005;102(43):15545–15550.
59. Liberzon A, Birger C, Thorvaldsdóttir H, Ghandi M, Mesirov JP, Tamayo P. The Molecular Signatures Database (MSigDB) hallmark gene set collection. *Cell Syst.* 2015;1(6):417–425.
60. Alamyar E, Duroux P, Lefranc MP, Giudicelli V. IMGT® tools for the nucleotide analysis of immunoglobulin (IG) and T cell receptor (TR) V-(D)-J repertoires, polymorphisms, and IG mutations: IMGT/V-QUEST and IMGT/HighV-QUEST for NGS. *Methods Mol Biol.* 2012;882:569–604.
61. Boca SM, Leek JT. A direct approach to estimating false discovery rates conditional on covariates. *PeerJ.* 2018;6:e6035.